Journal of Applied Polymer Science

"True" Biocomposites with Biopolyesters and Date Seed Powder: Mechanical, Thermal, and Degradation Properties

Vikas Mittal,[1] A. U. Chaudhry,[1] Nadejda B. Matsko[2]
[1]Department of Chemical Engineering, Petroleum Institute, Abu Dhabi, United Arab Emirates
[2]Graz Centre for Electron Microscopy, Graz, Austria
Correspondence to: V. Mittal (E-mail: vmittal@pi.ac.ae)

ABSTRACT: Biopolymers have gained research focus due to enhanced property profiles as well as need to replace the fossil fuel based polymeric materials. The generation of biocomposites with functional biofillers can lead to further enhancement of their potential. In this study, composites of date seed powder with biopolyesters poly(butylene adipate-co-terephthalate) (PBAT) and poly-L-lactide (PLA) have been demonstrated. The composites exhibited individual degradation peaks for the components in the thermogravimetric analysis (TGA), but still had suitable thermal performance confirmed by the dynamic TGA. The filler also modified the crystalline morphology of the polymers differently. The tensile modulus of the PBAT-based composites had enhancement of more than 300% in the composite with 40% filler content. The PLA composites also enhanced the modulus marginally till 20% filler content, however, it was still significant due to the very high modulus of PLA as compared to PBAT. The rheological properties indicated the polymer still had viscous behavior even when high amount of filler was added. The storage and loss modulus of the composites enhanced with filler fraction, the PLA composites with 30 and 40% content, however, exhibited very high values probably due to filler aggregates and low filler-polymer interfacial interactions. The filler particles were observed to be uniformly distributed in the polymer matrices, though some filler aggregates were also observed in the composites with higher filler fractions. After embedding in compost soil, the composites had significantly enhanced extent of biodegradation as compared to pure polymers, thus, confirming the "true" biocomposite nature. © 2014 Wiley Periodicals, Inc. J. Appl. Polym. Sci. **2014**, *131*, 40816.

KEYWORDS: biopolymers & renewable polymers; composites; rheology; properties and characterization

Received 24 January 2014; accepted 3 April 2014
DOI: 10.1002/app.40816

INTRODUCTION

Biopolymers (biobased and biodegradable) have become polymer matrices of interest in recent years.[1] The primary reason for their increased use is the fast depletion of fossil resources, which are the largest source of monomers used to synthesize majority of commercial polymers. In addition, these conventional polymers like polyolefins, polystyrene (PS), poly(methyl methacrylate), and so forth are non-biodegradable and recycling or reusing them is very challenging and costly. On the other hand, property profiles and processing methods associated with biopolymers have become more efficient and cost-effective over the years. In a recent study by Business Communications Company (BCC) Research, a significant compound annual growth rate of 22% for biodegradable polymers during the 5 year period starting from 2012 has been estimated.[2]

Incorporation of a large variety of fillers in the conventional polymers has been observed to result in significant enhancements in their mechanical, thermal, rheological, and gas barrier properties.[3–5] In order to generate high value materials from biopolymers, similar composites with fillers like layered silicates and nanotubes have also been reported.[6–8] Though the reported studies focused on the enhancement of mechanical properties of biopolymers on incorporation of fillers, the effect of filler on biodegradability of polymer has largely been ignored. In one study, a decrease in the biodegradation rate of the polymer in the presence of fillers has been reported,[9] thus, negating the positive effect of filler on other properties. Due to the "non-bio" nature of the filler phase used to generate such biocomposites, the composite material is not truly a biomaterial. Thus, by replacing such fillers with biofillers, it is possible to achieve the "true" biocomposite which would also retain (or enhance) the biodegradation characteristics of the polymer. However, the biofiller is required to play an active role in the composite structure (with positive interactions with polymer) rather than being passive filler added only to reduce cost.[10]

In this study, composites of biodegradable polyesters with date palm seed powder (DSP) have been generated with an objective

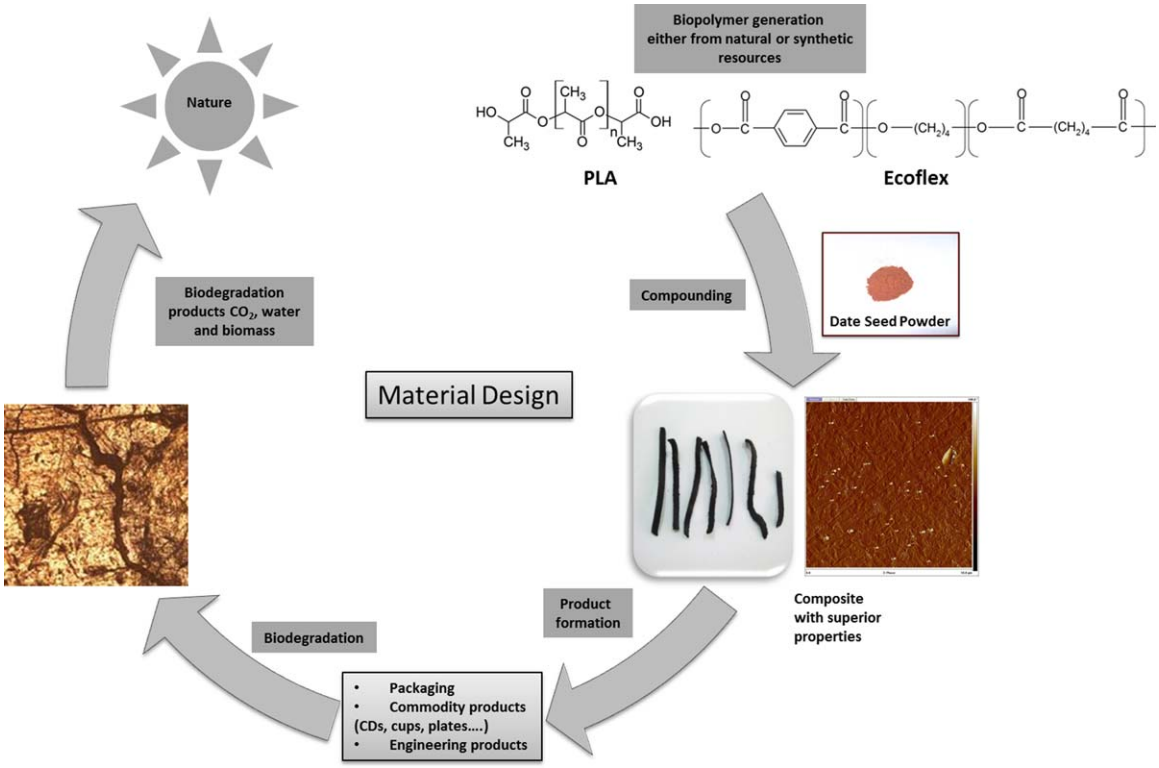

Scheme 1. Scheme demonstrating the design of eco-friendly composite materials. [Color figure can be viewed in the online issue, which is available at wileyonlinelibrary.com.]

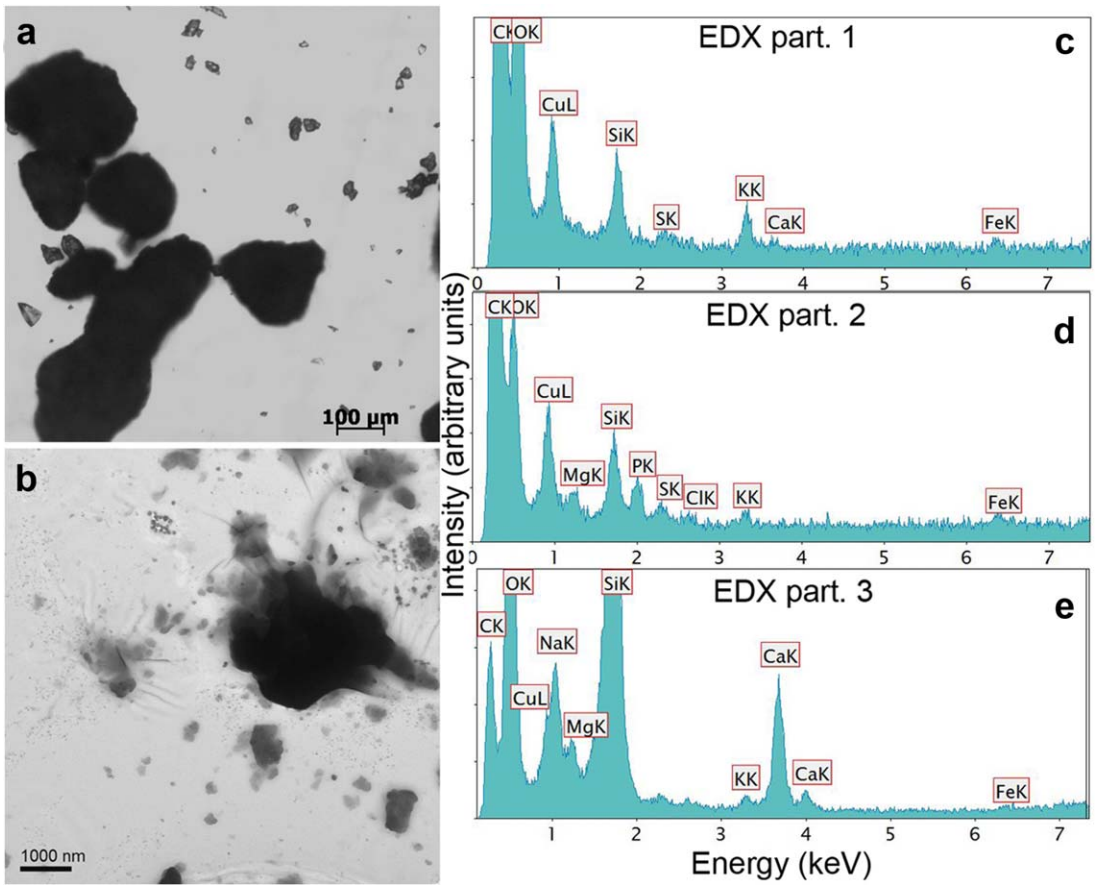

Figure 1. (a) Light microscopy image of DSP; (b) TEM image of the particles; (c–e) EDX analysis of the composition of DSP at three different locations on the TEM micrograph. [Color figure can be viewed in the online issue, which is available at wileyonlinelibrary.com.]

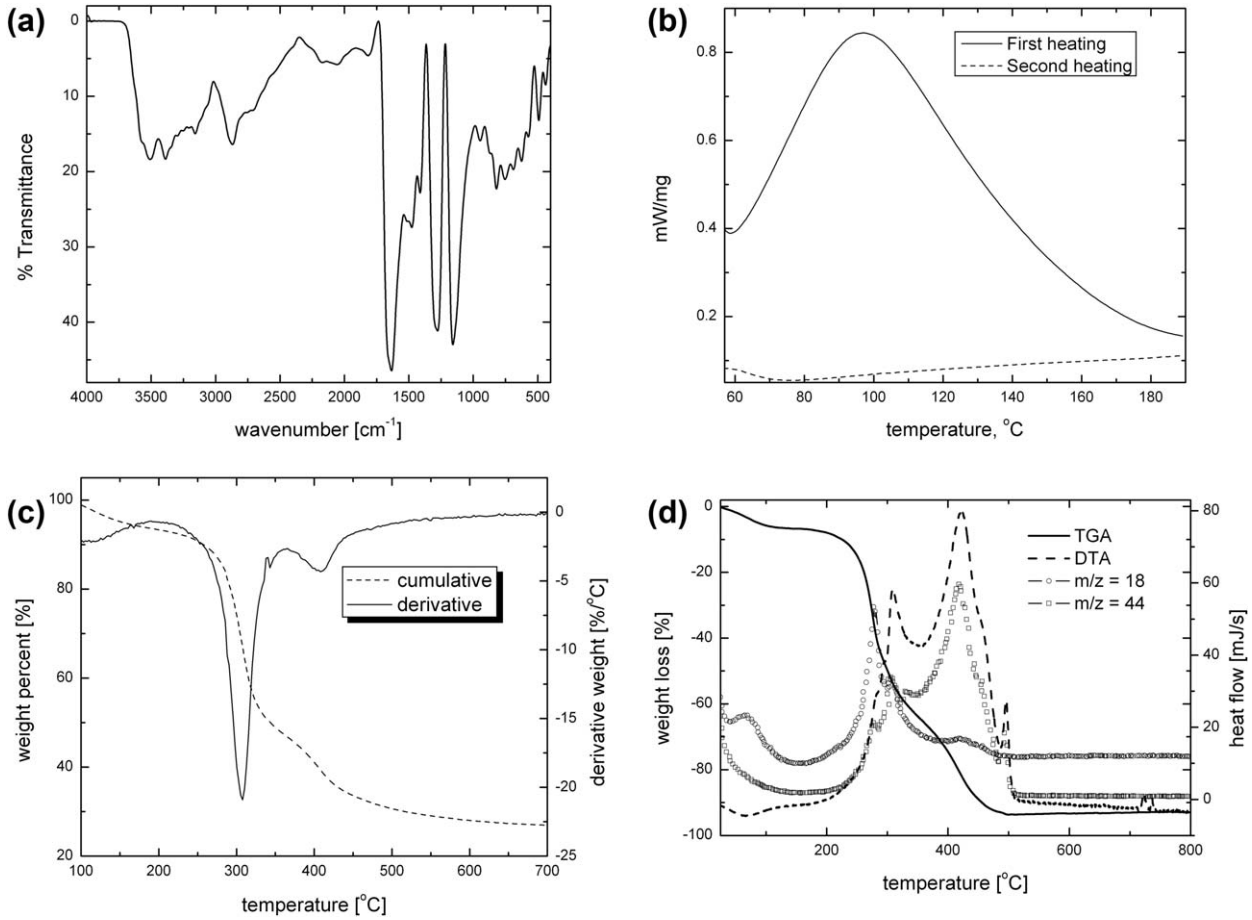

Figure 2. (a) FTIR spectrum of pure DSP; (b) DSC; (c) TGA (nitrogen) thermograms of pure DSP; (d) TGA-MS analysis of powder in air environment.

to achieve true biocomposites. The choice of filler was guided by the need of waste utilization due to the production of large amounts of date fruit in the Gulf region which leads to generation of significant amounts of seed waste. The biopolyester matrices chosen were poly(butylene adipate-co-terephthalate) (PBAT) and poly-L-lactide (PLA). These polymers were in rubbery and glassy state at room temperature, respectively, and the goal was to explore the effect of biofiller on their properties. In an earlier study on the use of DSP,[11] composites with high-density polyethylene (HDPE) and PS were reported using locally produced date pits "khlaas" and "sekari," which were wastes of two types of date palm fruit grown in Saudi Arabia. Reduction in mechanical properties of composites was observed and was attributed to a coarse morphology of the composite systems, especially in the absence of an appropriate coupling agent system. The glass transition temperature (T_g) of the PS/DSP composites and the heat of

Table I. Assignment of the Bands to the Constituents of DSP[19]

Band	Assignment
3500–3000 cm^{-1}	V_{OH} of hydroxyl and V_{NH} of protein
~2925 cm^{-1} & 2855 cm^{-1}	$V_{asy(CH2)}$ & $V_{sy(CH2)}$ of saturated fatty acids.
~1748 cm^{-1}	$V_{C=O}$ of ester carbonyl of fatty acids
1650–1500 cm^{-1}	$V_{C=O}$ & δ_{N-H} of proteins
~1455 cm^{-1}	$\delta_{asy(CH2)}$ & $\delta_{asy\ (CH3)}$ of saturated fatty acids and protein
~1380 cm^{-1}	$\delta_{asy(CH2)}$ & $\delta_{sy\ (CH3)}$ of saturated fatty acids and proteins. $V_{sy\ (C-O)}$ of COO-
~1250 cm^{-1}	V_{C-O} of ester carbonyls of fatty acids
1200–1000 cm^{-1}	δ_{OH} of hydroxyl and V_{C-O-C} of carbohydrates and its derivatives
~760 cm^{-1}	V_{CH} out of plane stretching of fatty acids

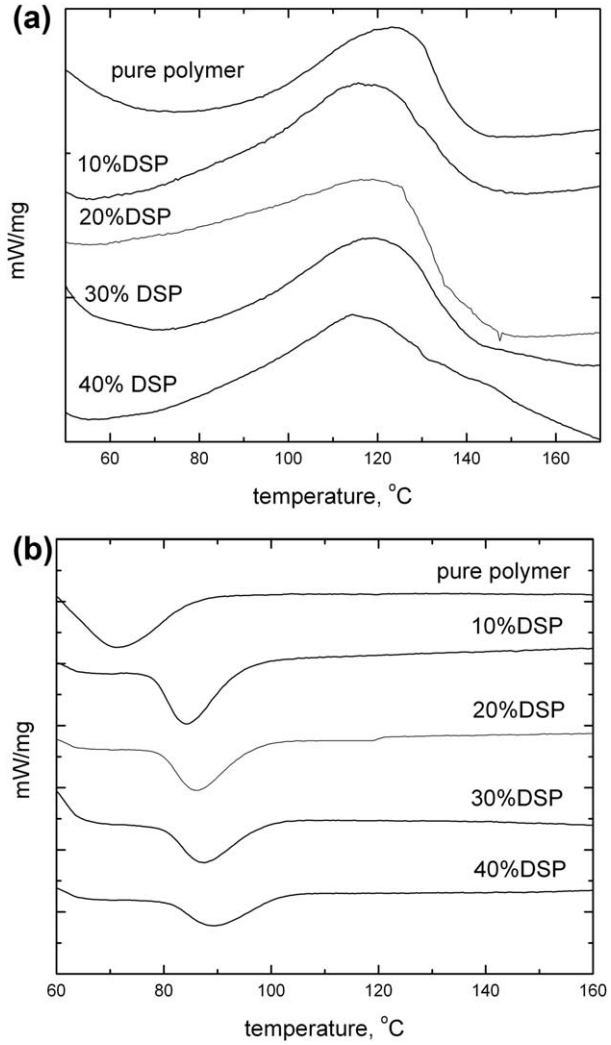

Figure 3. (a) Melting and (b) crystallization curves for PBAT and its composites with DSP.

fusion of the HDPE/DSP composites were observed to decrease at relatively higher powder content of >10 wt %. Ghazanfari et al.[12] reported the incorporation of DSP in HDPE and the melt flow index of the composites decreased whereas the thermal conductivity of the composites increased. The use of DSP in composites of recycled polypropylene was also reported and a decrease in the overall degree of polymer crystallinity with increasing powder content was observed.[13] A number of studies incorporating date fiber to generate fiber-reinforced composites have also been reported,[14–17] however, there is no reported study on exploring the effect of DSP on biopolymers. Thus, it is of importance to study extensively mechanical, rheological, thermal, and degradation properties of biopolymer-DSP composites as well as to correlate the obtained performance with the filler-polymer interaction, filler size as well as filler dispersion.

EXPERIMENTAL

Materials

Biopolyester PBAT with trade name Ecoflex® F Blend C1200 (density ~1 g/cm^3; melting range 100–130°C) was supplied by Badische Anilin and Soda Fabrik, Germany. It is a biodegradable aliphatic-aromatic copolyester based on the monomers 1,4-butanediol, adipic acid, and terephthalic acid in the polymer chain, which biodegrades to the basic monomers and eventually to carbon dioxide, water and biomass when metabolized in the soil or compost under standard conditions. PLA (procured from Biomer, Germany) with density 1.25 g/cm^3, T_g 50–60°C, and melting range 168–172°C was kindly provided by Prof. Misra at University of Guelph, Canada. Date seeds of Abu Dhabi region were procured locally.

Preparation of DSP

Fresh date seeds were cleaned with 50% H_2SO_4 for 5 h to remove the surface layers. The seeds were then cleaned with distilled water followed by drying. These were then milled in a ball mill and sieved using the 60 μm sieve in the shaker. The resulting powder with <60 μm fraction had fine morphology and was dark brown in color.

Preparation of Biocomposites

Biocomposites were prepared by melt mixing of DSP with biopolymers using mini-twin conical screw extruder (MiniLab Haake Rheomex CTW5, Germany). A mixing temperature of 145°C for PBAT and 190°C for PLA was used. The mixing was performed for 3 min at 80 rpm with batch size of 5 g. The screw length and screw diameter were 109.5 mm and 5/14 mm conical, respectively. Composites with filler content of 10, 20,

Table II. Calorimetric Properties of PBAT and PLA Composites[a]

	PBAT		PLA			
			First heating/cooling		Second heating/cooling	
Composite	Peak melting temp. (°C)	Peak crystallization temp. (°C)	Peak melting temp. (°C)	Peak crystallization temp. (°C)	Peak melting temp. (°C)	Peak crystallization temp. (°C)
Pure polymer	123	71	173	-	170	-
10% DSP composite	120	84	174	98	170	99
20% DSP composite	119	86	172	102	170	102
30% DSP composite	119	87	173	108	166, 172	109
40% DSP composite	115	90	172	110	165, 172	111

[a] Within ±1°C.

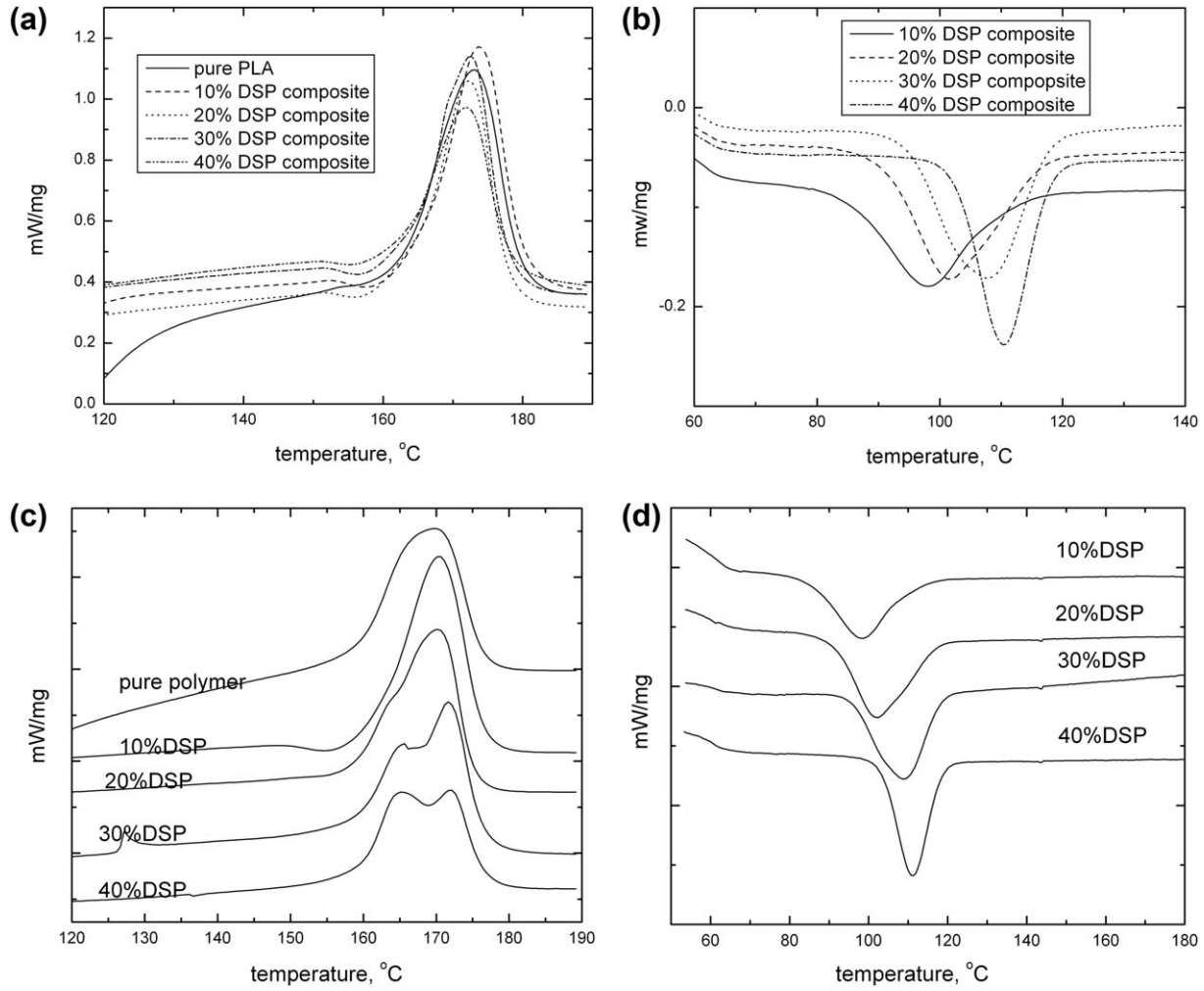

Figure 4. (a) Melting (first heating cycle) and (b) crystallization curves for PLA and its composites with DSP. Melting (second heating cycle) and corresponding crystallization curves are shown in (c) and (d), respectively.

30, and 40 wt % were generated. The disc and dumbbell-shaped test samples were prepared by mini-injection molding machine (Haake MiniJet, Germany) at processing temperatures of 145°C and 190°C for PBAT and PLA, respectively. The injection pressure was 700 bar for 6 s whereas holding pressure was 400 bar for 3 s. The temperature of the mold was kept at 55°C.

Characterization of the Composites

Thermal properties of the DSP, pure polymers, and biocomposites were analyzed using Netzsch thermogravimetric analyzer [TGA; using American Society for Testing and Materials (ASTM) standard ASTM E1131). Nitrogen was used as a carrier gas and the scans were obtained from 50 to 700°C at a heating rate of 20°C/min.

Linseis STA PT1600 TGA was also used to measure the weight change during heating in air atmosphere. This system is coupled with a Phipher mass spectrometer (MS) which allowed to determine H_2O ($m/z = 18$) and CO_2 ($m/z = 44$) elimination during heating. All measurements were realized with a heating rate of 3°C/min, using flow rate of 20 mL/min.

Calorimetric properties of the samples were recorded on a Netzsch differential scanning calorimeter (DSC) under nitrogen atmosphere (ASTM D3418-03). The scans were obtained from 50–190-50°C using heating and cooling rates of 15°C/min and 5°C/min, respectively.

Rheological properties of the biopolymers and composites such as storage modulus (G'), loss modulus (G''), viscosity (η'), and elasticity (η'') were measured on AR 2000 rheometer from TA Instruments (ASTM D4440). Disc shaped samples of 25 mm diameter and 2 mm thickness were characterized at 140°C for PBAT and 190°C for PLA using a gap opening of 1.2 mm. Frequency sweep scans (dynamic testing) of all PBAT composites were recorded at 1% strain from $\omega = 0.1$ to 100 rad/s, whereas a strain of 0.3% was used for PLA composites.

Tensile testing of pure polymers and biocomposites was performed on universal testing machine (Testometric, UK) using standard ASTM D638. The dumbbell shaped samples with 53 mm length, 4 mm width, and 2 mm thickness were used. A loading rate of 5 mm/min was employed and the tests were carried out at room temperature. WinTest Analysis software was

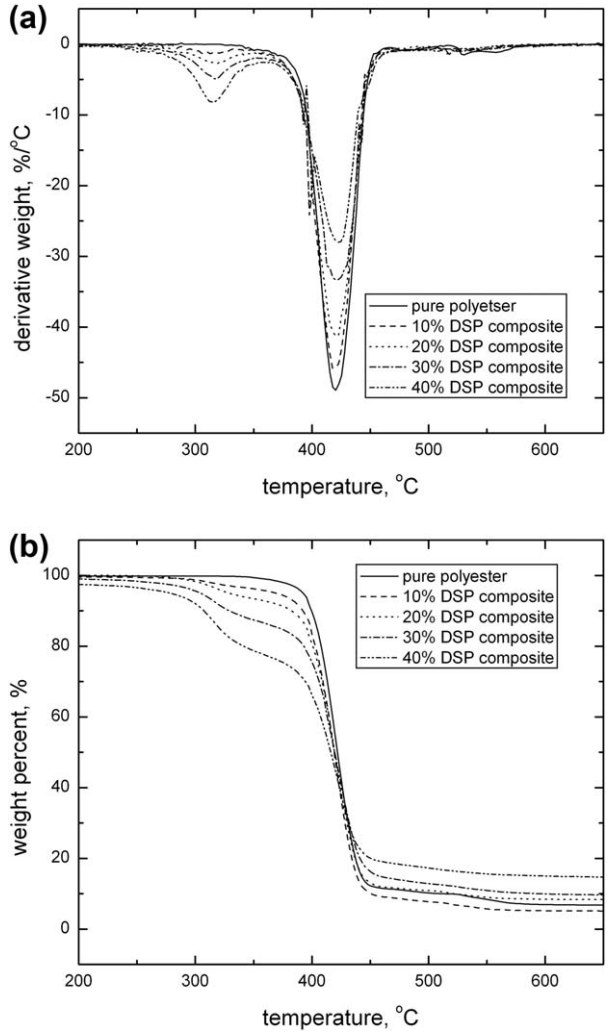

Figure 5. (a) Differential and (b) cumulative TGA thermograms of PBAT and composites.

used for the calculation of tensile modulus and other tensile properties. An average of five values is reported.

For the microscopy analysis, the composite samples were mounted in special holders which at the same time fit in the microtome and were suitable for the examination of the block face by atomic force microscopy (AFM). Ultrathin sections (30–90 nm) as well as block faces of the composite samples were obtained using a Leica Ultracut E microtome (Leica, Austria) equipped with a diamond knife (Diatome, Switzerland) at −120°C. Atomic force microscopy analysis of the block face of composites was obtained in tapping mode at ambient conditions using a Digital Instruments NanoScope III and silicon nitride cantilevers with natural frequencies in the 300 kHz range (force constant 20 N/m, tip radius 10 nm (NT-MDT, Russia). The block faces of specimens after cryo ultramicrotomy were also investigated at ambient conditions using ZEISS Axioplan light microscope (ZEISS, Germany) equipped with ZEISS Axio Cam ICc 1 CCD camera in reflected polarized light. Sections for transmission electron microscopy (TEM) analysis were collected on holy carbon coated 400 mesh electron microscopy grids, and were examined in a Philips CM 20 (Philips/FEI, Germany) electron microscope at 200 kV at room temperature without staining. TEM image processing was performed using DigitalMicrograph software (Gatan, USA). For TEM of DSP, the particles were adsorbed on carbon coated 400 mesh electron microscopy grids and were examined similarly as composites. All energy dispersive X-ray spectroscopy (EDXS) experiments were performed in scanning transmission electron microscopy mode with a probe current of 20 nA and a beam diameter of 100 nm, whereas EELS were performed in the TEM mode. EDXS spectra were collected using a HPGe detector (solid angle 0.13 sr). For the calculation of elemental distribution images, jump ratio method was used.[18]

Thermo Scientific Nicolet iS10 Fourier transform infrared (FTIR) spectrometer was used to study the IR spectrum of DSP (ASTM E1252). Pellet of DSP was pressed with KBr. Both absorbance and transmittance spectra in the wavenumber range of 4000–400 cm^{-1} were obtained.

Biodegradability of biopolymers and composites was analyzed by soil burial test under natural environmental conditions (ASTM

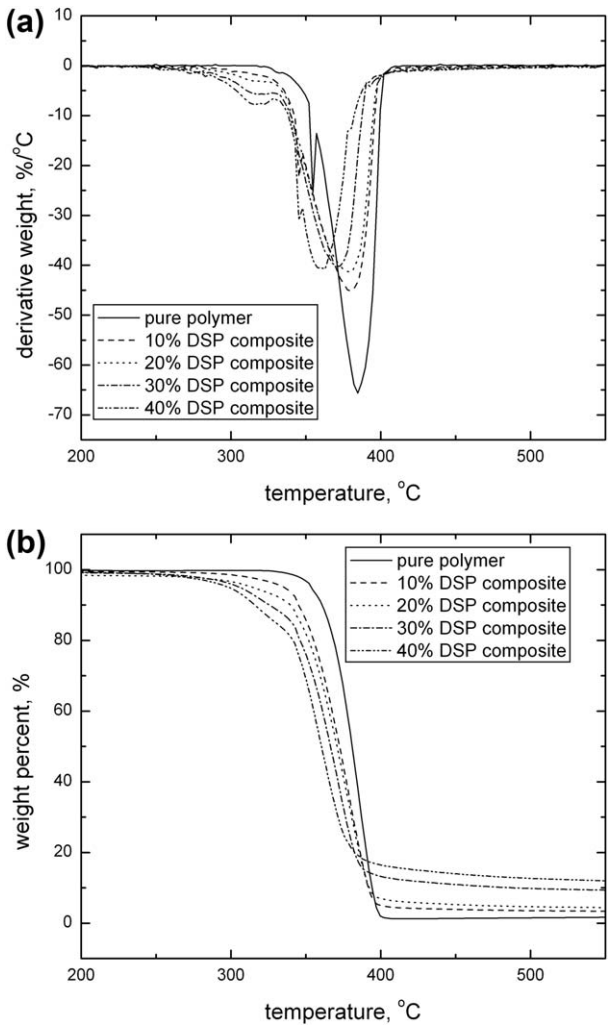

Figure 6. (a) Differential and (b) cumulative TGA thermograms of PLA and composites.

Table III. Mechanical Properties of the PBAT-DSP Composites (Average of 5 Measurements)

Composite	Tensile modulus[a] (MPa)	Yield stress[b] (MPa)	Yield strain[c] (%)	Stress at break[d] (MPa)	Total deformation[e] (mm)
Polymer	82.1	9.1	13.1	20.9	88.7
10% DSP composite	116.7	9.0	14.1	14.8	83.4
20% DSP composite	149.0	9.7	9.7	11.8	50.9
30% DSP composite	197.1	9.3	7.4	8.5	22.5
40% DSP composite	256.7	10.7	5.9	8.2	13.3

[a] Relative probable error 2%.
[b] Relative probable error 2%.
[c] Relative probable error 5%.
[d] Relative probable error 10%.
[e] Relative probable error 10%.

D6400). The samples were buried in open pots containing compost soil for gardening. Soil level in the pots was 10 cm, and the samples (with dimensions 15 × 10 × 1.5 mm^3) were buried 5 cm deep, 3.5 cm apart in longitudinal direction, and 4.5 cm apart in transverse direction. The soil moisture content varied in the range of 60–70%. The soil temperature was recorded in range of 33–37°C during the day and 20–25°C during night. The samples were dug out after 30, 60, and 120 days, washed and dried in a vacuum oven at 50°C followed by surface characterization in light microscope as well as weight loss analysis. The reported weight loss values represented an average of three samples.

RESULTS AND DISCUSSION

PBAT used in the study had similar properties as low density polyethylene because of its high molecular weight and long chain branched molecular structure. It had semi-crystalline morphology with a combination of properties like flexibility, process ability, utilization properties, and degradability. PLA, on the other hand, had much higher stiffness. Scheme 1 demonstrates the design of eco-friendly biocomposites along with applications and biodegradation.

Figure 1 shows the EDX analysis of the DSP. The particles had a different composition in the inner core and surface layer. Surface layer was observed to contain Si, Ca, and a variety of other elements. It was also obvious that the surface layer was not homogenized into a small dispersion and large particles in light microscopy and TEM images corresponded to this layer. Soft inner content contained mostly C, O, Si, and small amount of other elements. Therefore, the EDX spectra taken at different locations in the TEM micrograph had significant variations. FTIR spectrum of pure DSP in Figure 2(a) revealed the presence of fatty acid, carbohydrates, proteins, and water in DSP. Table I also demonstrates the assignment of absorption bands to the constituents.[19] The broad absorption between 3500 and 3000 cm^{-1} is attributed to —OH_{str} vibration of water and —NH_{str} vibration of proteins as well. Asymmetric and symmetric C—H stretching of methylene groups of saturated fatty acids are observed at 2925 cm^{-1} and 2855 cm^{-1}, respectively. The prominent bands present at 1748 cm^{-1} and 1250 cm^{-1} are attributed, respectively, to the C═O_{str} and C—O_{str} vibrations of ester carbonyls of fatty acids. The shoulder band between 1650 and 1500 cm^{-1} are corresponding C═O stretching and N—H bending of proteins. Bending vibrations of hydroxyl groups and C—O—C_{str} of carbohydrates could be observed between 1200 and 1000 cm^{-1}. The sharp absorbance around 760 cm^{-1} is attributed to C—H out of plane stretching of saturated fatty acids. In addition to these, elements like potassium, magnesium, calcium, phosphorous, sodium, and iron have also been reported to be part of the chemical composition of DSP.[20,21] DSC thermogram depicting

Table IV. Mechanical Properties of the PLA-DSP Composites (average of 5 measurements)

Composite	Tensile modulus[a] (MPa)	Yield stress[b] (MPa)	Yield strain[c] (%)	Stress at break[d] (MPa)
Polymer	3376	70.3	3.0	63.7
10% DSP composite	3528	53.5	2.2	43.7
20% DSP composite	3508	44.9	2.0	28.1
30% DSP composite	2495	7.3	0.3	16.3
40% DSP composite	2216	5.1	0.3	18.8

[a] Relative probable error 2%.
[b] Relative probable error 2%.
[c] Relative probable error 5%.
[d] Relative probable error 10%.

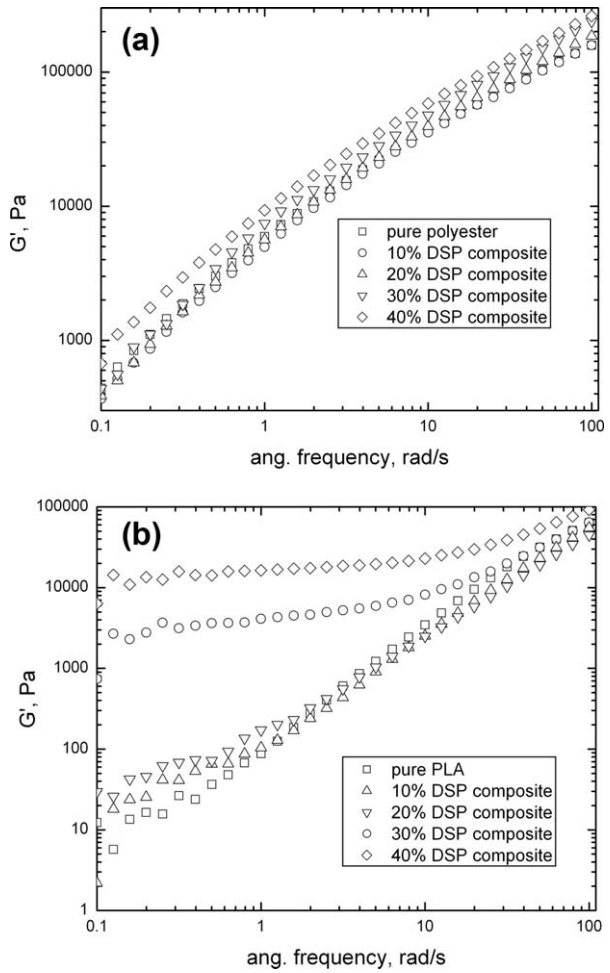

Figure 7. Storage modulus of (a) PBAT and (b) PLA composites as a function of filler content.

first heating in Figure 2(b) exhibited a broad endothermic transition with peak maximum at 100°C, however, the transition was completely absent in the second heating cycle. As the filler did not liquefy at higher temperature and as no crystallization peak was observed in DSC, the broad transition at 100°C can be attributed to the loss of moisture. It should also be noted that the oil is extracted from DSP when it is subjected to high temperature conditions (180–200°C).[21] This may also be the reason of differences in the first and second heating cycles in the DSC. Generation of oil inside the composite matrix can also lead to further effects, for example, composite flexibility as well as oil migration within the matrix. The TGA thermogram (in nitrogen) of DSP in Figure 2(c) also indicated a weight loss of ~10% in the temperature range of 50–200°C probably due to loss of moisture, indicating that the powder had large amount of moisture content. This phenomenon was retained even though the powder was dried overnight at 60°C under vacuum, which indicated that the moisture may not be present only on the surface of particles, but more tightly bound in the structure. To further confirm if the observed TGA transitions corresponded to moisture loss (or to degradation products of DSP), Figure 2(d) shows the TGA-MS analysis of the pure seed powder. Air was used as analysis medium to simulate the actual processing environment used for generation of composites. Weight loss in the region of 50–200°C was attributed to MS curve corresponding to $m/z = 18$, which confirmed the loss of moisture responsible for the weight loss. Degradation at higher temperature led to the evolution of carbon dioxide along with water as evident from MS curves corresponding to $m/z = 44$ and $m/z = 18$. Though the degradation behavior of the powder was different in nitrogen and air environments, the peak degradation was observed to take place at ~300°C which confirmed the suitability of DSP for melt mixing with polymers at high temperatures under shear. Interestingly, the powder did not lose weight completely even at 700°C.

Figure 3 shows the melting and crystallization thermograms of PBAT and its composites. The peak melting and crystallization temperatures are also reported in Table II. As compared to a peak crystallization temperature of 71°C for pure polymer, a significantly higher value of 90°C was observed for 40% DSP composite. The peak melting point was, however, observed to reduce as the fraction of DSP was enhanced, though the effect was not as significant as the increment in peak crystallization

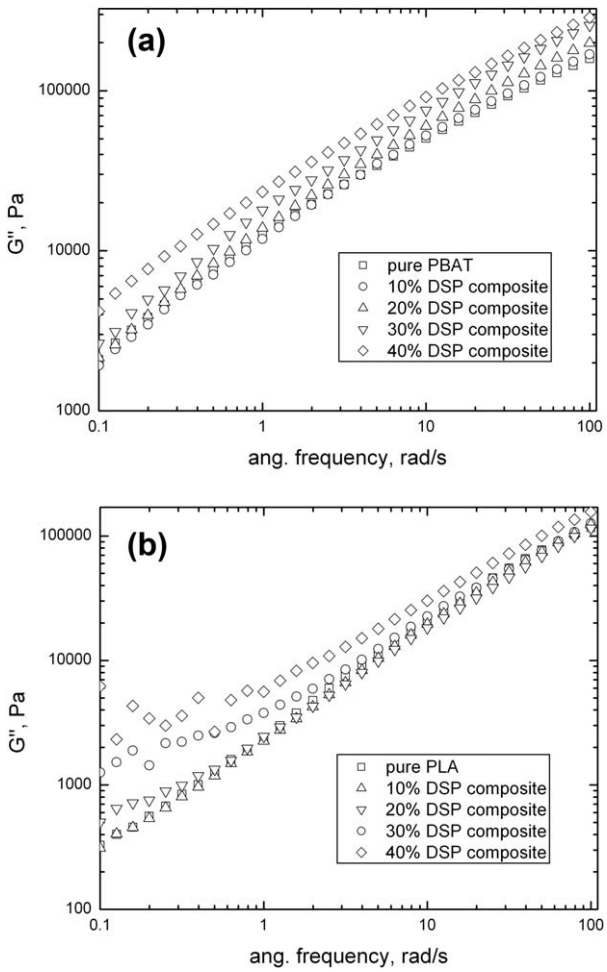

Figure 8. Loss modulus of (a) PBAT and (b) PLA composites as a function of filler content.

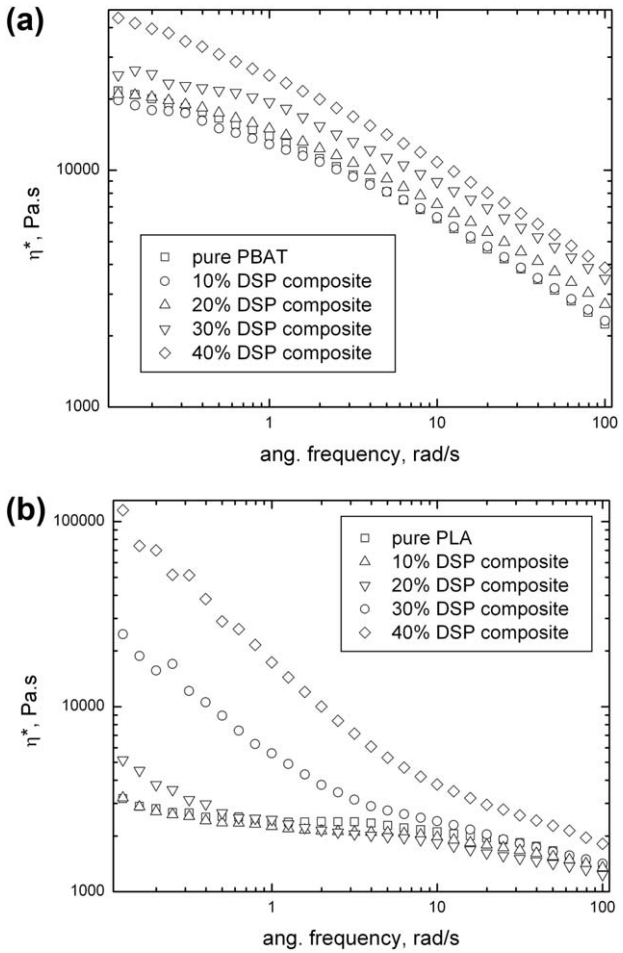

Figure 9. Complex viscosity of (a) PBAT and (b) PLA composites with increasing amount of DSP.

temperature. Crystallization enthalpy (normalized to amount of pure polymer in the composite) was also observed to decrease as a function of increasing filler content in the polymer. For example, in comparison to a value of 22.7 J/g for pure polymer, composite with 40% DSP exhibited a value of 14.5 J/g for crystallization enthalpy. Figure 4 (and Table II) shows the similar DSC analysis for the PLA composites. Pure PLA did not crystallize in the cooling conditions used, however, the peak crystallization temperature in the composites increased on increasing the filler content. Contrary to PBAT behavior, the melting point did not change in the PLA composites as it lied in the range from 172 to 174°C. Crystallization enthalpy also increased on increasing filler content indicating that the filler enhanced the overall crystallinity in the PLA composites. In order to eliminate the effect of thermal history in PLA, second heating and crystallization runs were performed to confirm the findings in the first heating and crystallization cycles. As shown in Figure 4(c,d), the crystallization behavior of the polymer was similar to the first cycle, however, the melting behavior showed variations as compared to the first cycle especially at higher filler content. The composites with 20–40% DSP showed two distinct melting transitions, the magnitude of the lower temperature signal increased on increasing the filler content. The higher temperature peak coincided with the melting point of the pure polymer, whereas the low temperature peak may have resulted from the smaller sized crystals or different crystal forms which formed especially when the content of the filler increased in the matrix. The crystallization enthalpy similarly increased as the DSP content was enhanced confirming the enhancement of overall crystallinity of PLA.

Figures 5 and 6 demonstrate the TGA (nitrogen) thermograms of PBAT and PLA composites. Degradation signals with peak values around 300°C, corresponding to the degradation of pure DSP, were observed in the composites and the magnitude of the degradation increased corresponding to the fraction of the filler in the composites. This indicated that DSP was not mixed with the polymers at molecular level, which otherwise would have resulted in a single degradation peak for the composites. Such a phenomenon is expected due to the coarse size of the date seed particles. The peak degradation temperature in the PBAT composites did not change as compared to pure polymer, however, it was observed to decrease in the PLA composites as a function of filler fraction. As compared to pure PLA, a decrease of 20°C was

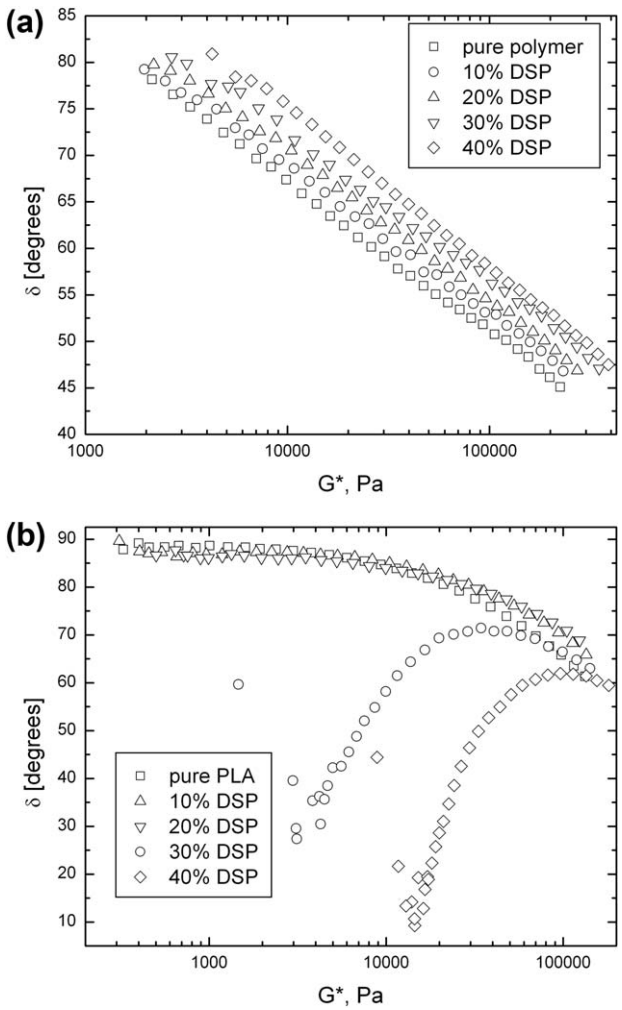

Figure 10. van Gurp compatibility analysis for (a) PBAT and (b) PLA composites.

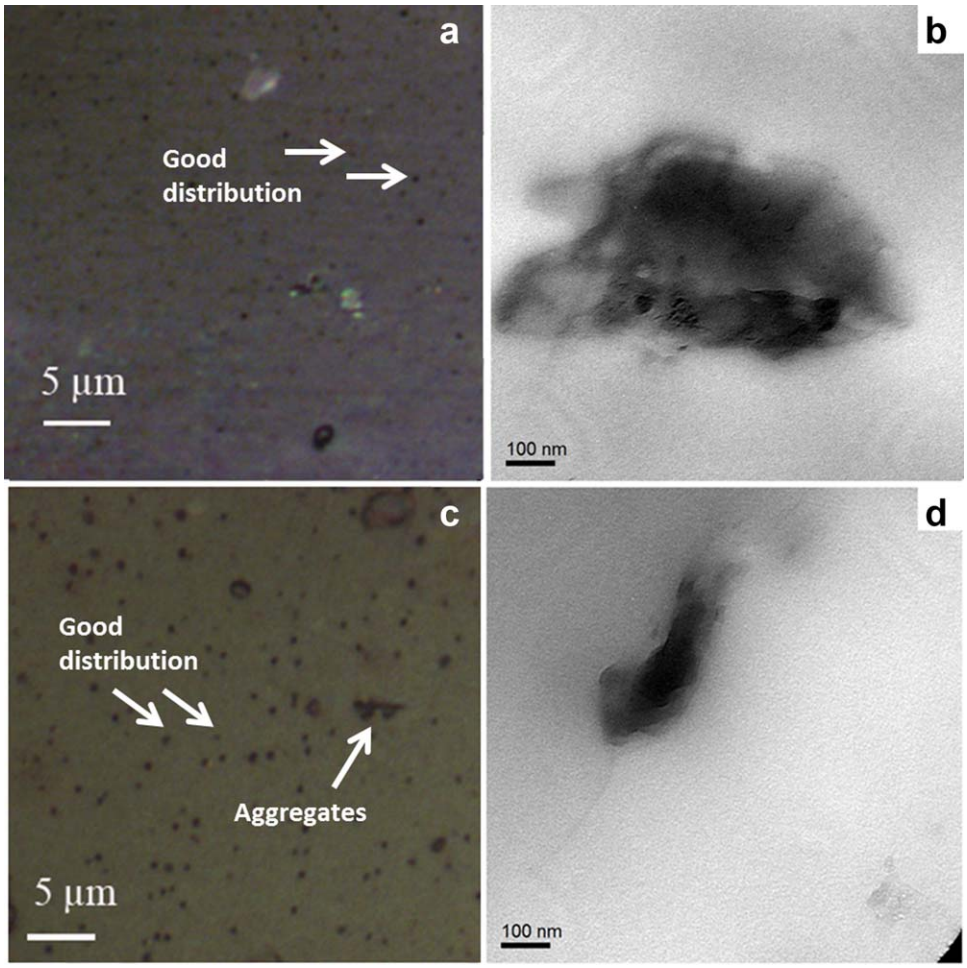

Figure 11. (a) Light microscopy and (b) TEM images of PBAT composite with 10% DSP content. (c) and (d) correspond to light microscopy and TEM images of PBAT composite with 30% DSP content. The dark phase in these images represents the cross-section of filler particles. [Color figure can be viewed in the online issue, which is available at wileyonlinelibrary.com.]

observed in the peak degradation temperature in the composite with 40% DSP content. This indicated that the thermal performance of the PLA composites reduced on addition of DSP, however, the degradation still occurred at temperatures much higher than the processing temperatures used for commercial applications. Dynamic TGA runs were also performed by equilibrating the composite samples at compounding temperature in order to ascertain the time the sample remained thermally stable. The composites did not lose 1% organic mass even after 5 min (as compared to 3 min compounding time), which confirmed the thermal stability for the commercial applications.

The tensile modulus of the PBAT composites was observed to increase significantly as the fraction of filler was enhanced (Table III). The modulus for the pure polymer was 82 MPa, which was enhanced to 257 MPa for composite with 40% DSP, thus, registering an increase of more than 300% and also confirming efficient stress transfer from the polymer to filler particles. Moreover, though the TGA indicated that the polymer and filler phases were not mixed at molecular level, but the observed enhancements in the modulus cannot be achieved without good filler dispersion. It should also be noted that the enhancement in the modulus was observed even though overall crystallinity decreased in PBAT composites. It is expected that the filler particles resulted in uniformity in the crystal size distribution which helped to enhance the overall mechanical performance. For the same reason, the yield stress was also marginally enhanced from 9.1 MPa for pure polymer to 10.7 MPa for composite with 40% DSP. The yield strain (and overall elongation) was observed to decrease owing to strain hardening of the chains due to the presence of large number of filler particles. The coarse size of the filler particles also led to the reduction in the stress at break value of the composites. As expected, the reduction was much more significant in composites with 30% and 40% fraction of filler. Table IV demonstrates the mechanical performance of PLA composites. The modulus of PLA enhanced to 3528 MPa on incorporating the matrix with 10% filler as compared to 3376 MPa for pure polymer, however, the modulus decreased on further enhancing the filler content. It should be noted that as PLA itself had very high tensile modulus, thus, enhancement of modulus even marginally by adding biofiller indicated the potential of DSP as

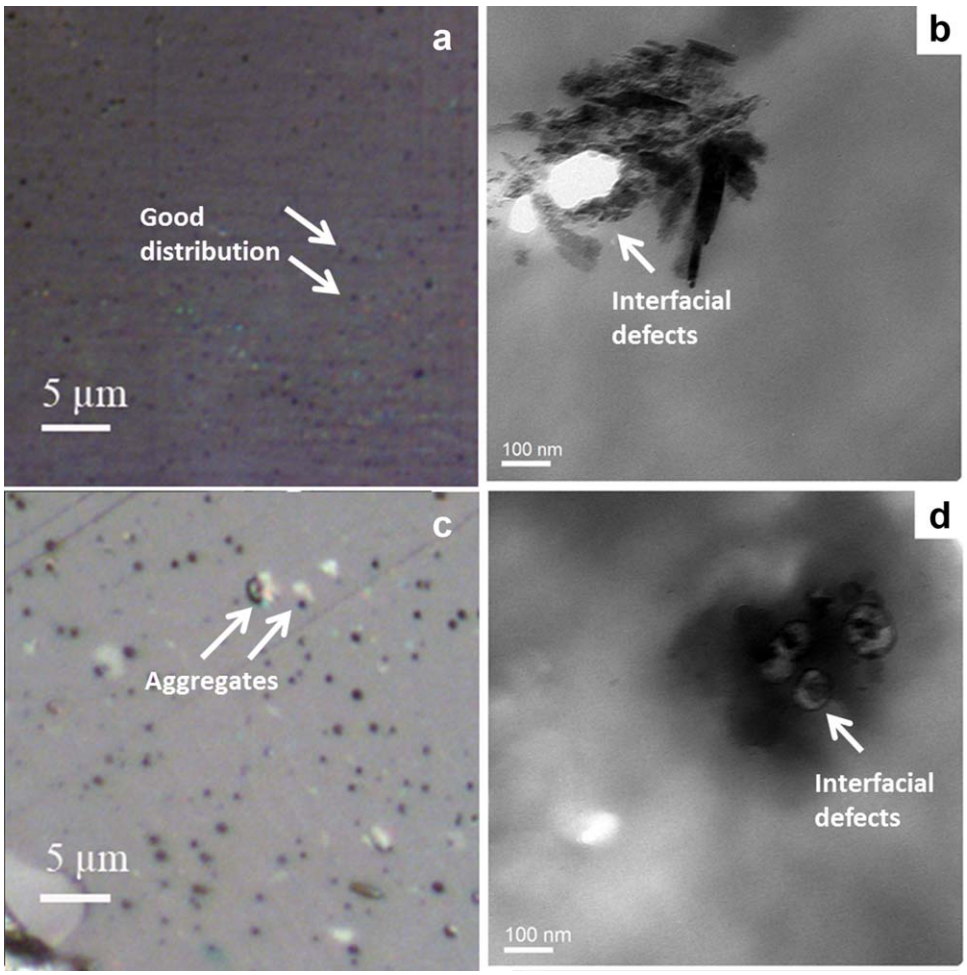

Figure 12. (a) Light microscopy and (b) TEM images of PLA composite with 10% DSP content. (c) and (d) correspond to light microscopy and TEM images of PLA composite with 30% DSP content. The dark phase in these images represents the cross-section of filler particles. [Color figure can be viewed in the online issue, which is available at wileyonlinelibrary.com.]

functional filler. The reduction in modulus was very significant in 30% and 40% filler composites indicating that the higher contents of filler led to stress concentration in already brittle matrix. Enhanced polymer crystallinity in the presence of DSP would have also contributed further to this effect. The other mechanical properties also decreased in the composites, however, the reduction was extensive in the composites with 30% and 40% DSP content. The comparison of mechanical performance of the composites also indicated that the interfacial interactions in PBAT composites were better than the corresponding PLA composites.

Network structure of the polymer composites was evaluated with shear rheology and the storage and loss moduli of the samples as a function of angular frequency are demonstrated in Figures 7 and 8. The storage modulus of the pure polymers was lowest at all frequencies. The modulus increased on increasing angular frequency, but the rate of increase in modulus decreased on increasing the frequency. In the case of PBAT composites, the composites with 10 and 20 wt % filler content had similar storage modulus, the higher filler fraction enhanced gradually the modulus values [Figure 7(a)]. For example, at an angular frequency of 10 rad/s, the storage modulus for PBAT was 36,470 MPa, which was enhanced to 50,530 MPa for composite with 40% filler content. In the case of PLA composites [Figure 7(b)], the composites with 10% and 20% filler content had similar storage modulus as the pure polymer at higher frequencies. At lower angular frequencies, the modulus increased with increasing filler content. The composites with 30% and 40% filler fraction, however, had very different behavior as indicated by their significantly high storage modulus values especially at lower frequencies. At higher frequencies, though the trends were maintained, the magnitude of the deviation was reduced. As discussed earlier, presence of large sized filler particles and non-interaction at the polymer-filler interface may lead to such hindrance to the melt shearing process. Such morphology could also be related to the observed significant reduction in the tensile properties of the composites. Figure 8(a) demonstrates the loss modulus of the pure PBAT and corresponding composites. The loss modulus curves exhibited similar trends as the storage

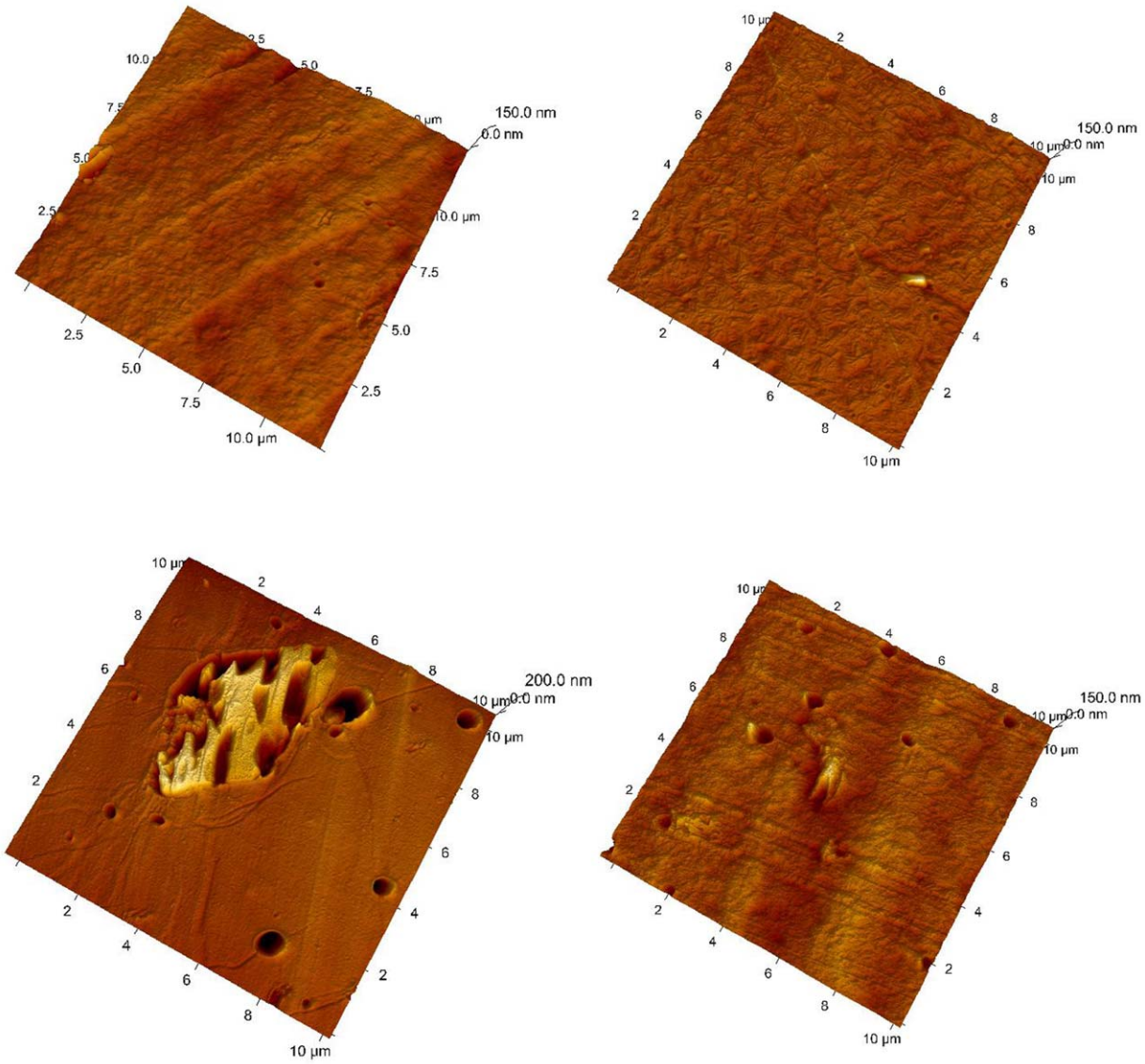

Figure 13. AFM height micrographs of PBAT composites with (top left) 10% and (bottom left) 30% DSP content; micrographs of the PLA composites with (top right) 10% and (bottom right) 30% DSP content. [Color figure can be viewed in the online issue, which is available at wileyonlinelibrary.com.]

modulus. For example, at 10 rad/s angular frequency, the composite with 40% DSP content had loss modulus values of 91,230 MPa as compared to 58,390 MPa for pure polymer. On comparison with the storage moduli of the composites, it was observed that in pure PBAT as well as all the composites, G'' was always higher than G' at any angular frequency. It indicated that the morphology of the samples had dominant viscous behavior with long relaxation times. In the case of loss modulus of PLA composites shown in Figure 8(b), the composite with 20% filler content exhibited a slightly higher modulus value than pure polymer only at lower frequency. Composites with 30% and 40% filler content had significantly higher loss moduli at lower frequencies, but the curves tended to merge with other composites at higher frequencies. Similar to PBAT composites, G″ was always higher than G′ for PLA and its composites till 20% DSP content. For composites with higher DSP content, the behavior had elastic dominance at lower angular frequency.

Similar to shear moduli, η' (viscosity) $> \eta''$ (elasticity) was true for PBAT as well as its composites at all angular frequency values indicating that the viscous contribution dominated the effect of elasticity in these samples. The η'' curves for PBAT systems exhibited an increase in elasticity till a frequency of 1 rad/s followed by gradual decrease at higher frequencies. It is possible that at lower frequency, the entanglements and interactions between the filler and polymer exhibited elastic behavior, but at higher frequencies, these did not withstand the shear. The generation of oil from the filler particles at higher shear (or angular frequency) would also lead to reduction in the elasticity in the composites.[21] In the case of PLA composites, $\eta' > \eta''$ was also

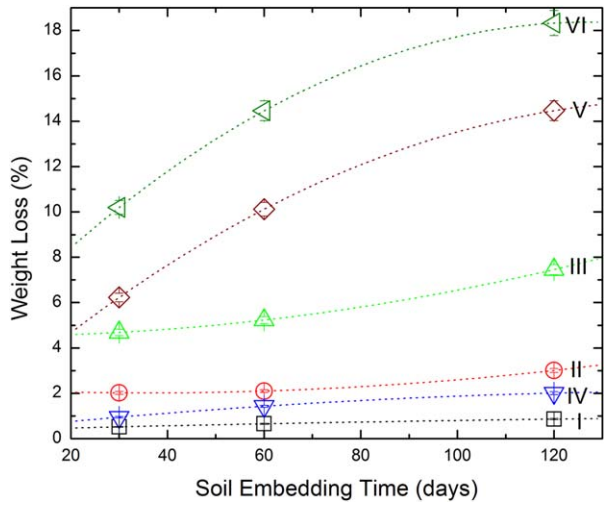

Figure 14. Weight loss versus soil embedding time for PLA, PBAT and composites. I: PLA; II: PLA + 20%DSP; III: PLA + 40%DSP; IV: PBAT; V: PBAT + 20%DSP; VI: PBAT + 40%DSP. [Color figure can be viewed in the online issue, which is available at wileyonlinelibrary.com.]

true for the polymer and its composites till 20% DSP content and at higher frequency for composites with higher filler content, thus, confirming the dominance of the viscous contribution. Similar to PBAT, the elasticity in the case of pure PLA and composites with 10 and 20 wt % filler content increased marginally at lower frequency probably due to network of entanglements. However, the composites with higher filler content had a significant decrease in this value due to poor interface between the filler and polymer due to large amount of filler particles leading to stress concentration. This also justified the poor tensile performance observed earlier for these composites as well as higher friction due to coarse particles leading to higher values of storage modulus. The combined effect of viscosity and elasticity of the polymers and composites is demonstrated in the form of complex viscosity in Figure 9.

Though the commonly used Cole-Cole,[22–24] van Gurp,[25,26] and Han Chuang[27,28] criteria to determine phase miscibility are applicable for polymer blends, some literature studies have also reported the advantages of these criteria for polymer composite systems.[25,29] Figure 10 shows the van Gurp plots representing the relationship between complex modulus (G^*) and phase angle (δ). The merging of the data to a single curve represents a compatible system. In the case of PBAT composites [Figure 10(a)], the curves did not merge to a single curve, however, deviated gradually as the filler content was increased indicating gradual reduction in compatibility as the filler content was enhanced. In PLA composites [Figure 10(b)], the time-temperature superposition principle was observed to hold till 20% filler content as indicated by the merging of the curves into a common curve. The composites with 30% and 40% content deviated extensively from the common curve thus confirming the presence of extensive immiscibility in these samples. It also indicated that extent of immiscibility in this case was higher than the PBAT composites. The curves of PLA composites with higher filler fractions almost converged with each other at higher frequency (lower δ value), however, they still did not merge to a common curve. The miscibility studies thus demonstrated that the polymer composites had phase miscibility when lower extents of filler were added. Addition of higher filler

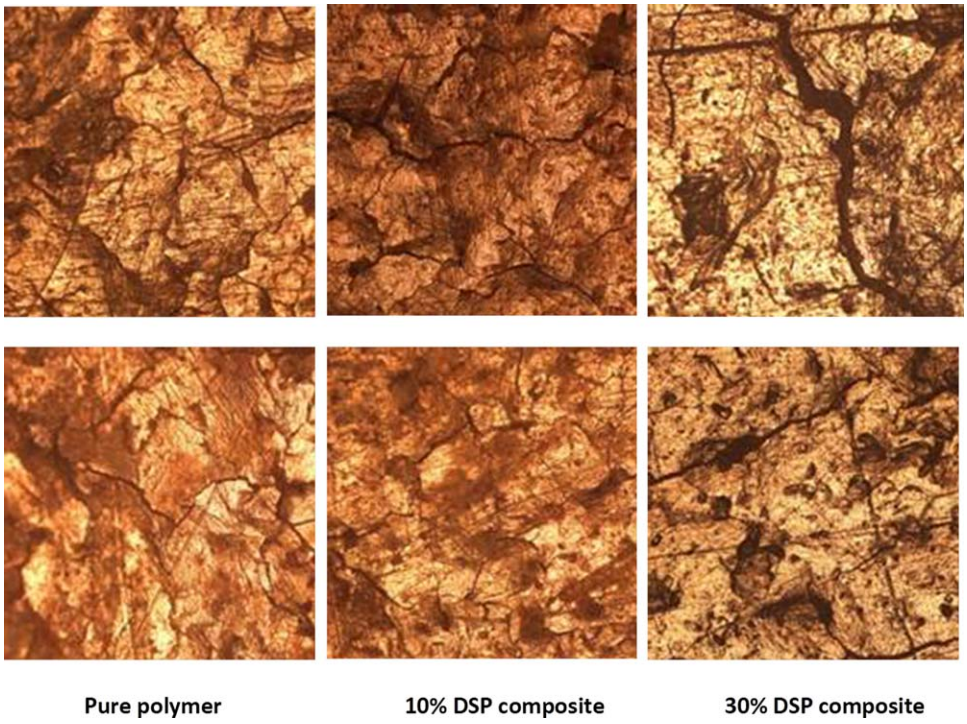

Figure 15. Optical micrographs of (upper row) PBAT and (lower row) PLA and their composites after embedding into natural soil for 120 days. The width of images reads 100 μm. [Color figure can be viewed in the online issue, which is available at wileyonlinelibrary.com.]

amount led to generation of phase immiscibility in the composites, however, the magnitude of immiscibility was extensive in the case of PLA composites. Poor interface between the PLA chains and filler surface due to presence of coarse filler particles acting as stress concentration points would have resulted in such a behavior.

Figure 11(a,c) show the light microscopy images of the PBAT composites with 10% and 30% DSP content. The date seed particles were observed to be uniformly distributed (dark particles) in the polymer matrices, though the size distribution of these particles was broad. Occasionally, especially in composites with 30 wt % filler content, filler aggregates were also observed. The TEM images at high resolution exhibited good adhesion at particle-matrix interface as no void or particle pull-out was observed during sectioning. This can also be attributed to result in significant improvement of the mechanical characteristics. Figure 12 also demonstrates similar analysis for PLA composites. The TEM images exhibited some defects at the filler-polymer interface [Figure 12(b,d)], which also confirmed the earlier findings from the mechanical analysis. Figure 13 also demonstrates the AFM height images of the PBAT and PLA composites with 10% and 30% DSP. The polymers had significantly different phase morphology. Similar to optical micrographs, filler particles with broad size distribution were also visible especially in the composites with 30% filler content. Interestingly, the composites were also observed to have voids at the surface, the magnitude and size of which was much higher when the filler content was higher. This effect was linked to filler and its content only, as no such voids were observed in the pure polymers. As DSP loses extensive moisture at the compounding conditions, one possible cause of such voids was due to the escape of high temperature steam from the matrix, however, further analysis would be required to confirm this hypothesis. Such micro-channels in the matrix can be of immense benefit in certain applications related to migration of gases or other materials through the polymer.

Quantitative studies on biodegradation of the composites were also performed in order to analyze the effect of DSP on biodegradation. As shown in Figure 14, addition of DSP to biopolyesters enhanced the biodegradation as a function of embedding time and filler content. The pure polymers had minimal degradation even after 120 days of embedding, whereas the composites exhibited higher extents of degradation. PBAT composites had higher degree of degradation as compared to PLA composites confirming the effect of DSP in ensuring the formation of true biocomposites. Also, as shown in Figure 15, the pure polymers after embedding for 120 days in composting soil exhibited surface roughness as well as micro-cracks indicating initiation of degradation of polymer structure. The extent of cracking was observed to enhance in the composites with 10% DSP content (especially in PBAT). The composites with 30% DSP content further exhibited widened cracks along with surface degradation.

CONCLUSIONS

True biocomposites with biopolyesters PBAT and PLA as polymer matrices and DSP were successfully manufactured. The DSP was observed to be thermally stable at the processing temperatures and had polar hydroxyl and carboxyl groups on the surface. The melting point in the PBAT composites decreased as a function of DSP content, which remained constant in the PLA composites. The onset and peak crystallization temperatures in the composites increased as increasing filler fraction. The overall crystallinity decreased in PBAT composites, whereas opposite effect was observed in PLA composites. The tensile modulus of the PBAT was significantly enhanced by incorporation of DSP and showed enhancement even at 40% filler content indicating good filler-polymer interaction. The PLA composites, on the other hand, had tensile modulus enhancement till 20% filler content, after which the modulus reduced significantly probably due to poor filler-polymer interfacial interactions and coarse size of particle leading to stress concentration. The other tensile properties in PBAT composites were either same as polymer or had marginal reduction, but the reduction was much more significant in PLA composites. The storage and loss moduli of the composites gradually increased with filler content, but the PLA composites with higher filler content had significantly higher values probably due to hindrance to shear by larger sized filler particles in the absence of interactions with polymer. The polymer in the composites also had dominant viscous character. The optical microscopy confirmed good distribution of filler particles in the polymer matrices, but filler aggregates in the composites with higher filler content were also observed. The composites exhibited better biodegradation as compared to pure polymers thus confirming that DSP enhanced the biodegradation and formed true biocomposites.

ACKNOWLEDGMENTS

The authors are indebted to Dr. Gisha Luckachan at The Petroleum Institute for the IR analysis.

REFERENCES

1. Averous, L.; Boquillon, N. *Carbohydr. Polym.* **2004**, *56*, 111.
2. BCC Research Report, Available at: http://www.bccresearch.com/report/biodegradable-polymers-market-pls025d.html.
3. Mark, J. E. *Polym. Eng. Sci.* **1996**, *36*, 2905.
4. Mittal, V. *J. Thermoplastic Compos. Mater.* **2007**, *20*, 575.
5. Chaudhry, A. U.; Mittal, V. *Polym. Eng. Sci.* **2013**, *53*, 78.
6. Ray, S. S.; Yamada, K.; Okamoto, M.; Ueda, K. *Polymer* **2003**, *44*, 857.
7. Sinha Ray, S.; Bandyopadhyay, J.; Bousmina, M. *Polym. Degrad. Stab.* **2007**, *92*, 802.
8. Favier, V.; Canova, G. R.; Shrivastava, S. C.; Cavaille, J. Y. *Polym. Eng. Sci.* **1997**, *37*, 1732.
9. Wu, T.-M.; Wu, C.-Y. *Polym. Degrad. Stab.* **2006**, *91*, 2198.
10. Suryanegara, L.; Nakagaito, A. N.; Yano, H. *Compos. Sci. Technol.* **2009**, *69*, 1187.
11. Alsewailem, F. D.; Binkhder, Y. A. *J. Reinforced Plast. Compos.* **2010**, *29*, 1743.

12. Ghazanfari, A.; Emami, S.; Panigrahi, S.; Tabil, L. G. *J. Compos. Mater.* **2008**, *42*, 77.
13. AlMaadeed, M. A.; Kahraman, R.; Khanam, P. N.; Madi, N. *Mater. Des.* **2012**, *42*, 289.
14. Mahmoudi, N.; Hebbar, N. *J. Compos. Mater.* **2014**, *48*, 2910299.
15. Ibrahim, H.; Farag, M.; Megahed, H.; Mehanny, S. *Carbohydr. Polym.* **2014**, *101*, 11.
16. Shalwan, A.; Yousif, B. F. *Mater. Des.*, **2014**, *53*, 928.
17. Mahmoudi, N. *Mech. Ind.* **2013**, *14*, 71.
18. Hofer, F.; Warbichler, P. *Ultramicroscopy* **1996**, *63*, 21.
19. Mahapatra, D. M.; Ramachandra, T. V. *Curr. Sci.* **2013**, *105*, 47.
20. Nehdi, I.; Omri S.; Khalil, M. I.; Al-Resayes, S. I. *Ind. Crop. Prod.* **2010**, *32*, 360.
21. Besbes, S.; Blecker, C.; Deroanne, C.; Drira, N. E.; Attia, H. *Food Chem.* **2004**, *84*, 577.
22. Cho, K.; Lee, B. H.; Hwang, K. M.; Lee, H.; Choe, S. *Polym. Eng. Sci.*, **1998**, *38*, 1969.
23. Kim, H. K.; Rana, D.; Kwag, H.; Choe, S. *Korea Polym. J.* **2001**, *8*, 34.
24. Kwag, H.; Rana, D.; Choe, K.; Rhee, J.; Woo, T.; Lee, B. H.; Choe, S. *Polym. Eng. Sci.*, **2000**, *40*, 1672.
25. Joshi, M.; Butola, B. S.; Simon, G.; Kukaleva, N. *Macromolecules* **2006**, *39*, 1839.
26. van Gurp, M.; Palmen, J. *Rheol. Bull.* **1998**, *67*, 5.
27. Chuang, H. K.; Han, C. D. *J. Appl. Polym. Sci.* **1984**, *29*, 2205.
28. Han, C. D.; Chuang, H. K. *J. Appl. Polym. Sci.* **1985**, *30*, 4431.
29. Ahmed, J.; Varshney, S. K.; Auras, R. *J. Food. Sci.* **2010**, *75*, 17.